Author Manuscript

Authors: Atanu Banerjee; Jia Li; Amy L. Speelman; Corey J. White; Piotr L. Pawlak; William W. Brennessel; Nicolai Lehnert; Ferman A Chavez

A Structural Model for the Iron-Nitrosyl Adduct of Gentisate Dioxygenase

Atanu Banerjee,[a] Jia Li,[a] Amy L. Speelman,[b] Corey J. White,[b] Piotr L. Pawlak,[a] William W. Brennessel,[c] Nicolai Lehnert,[b] and Ferman A. Chavez*,[a]

[a]Department of Chemistry, Oakland University, Rochester, MI 48309-4477, USA,

E-mail: chavez@oakland.edu, https://files.oakland.edu/users/chavez/web/Research.htm

[b]Department of Chemistry, The University of Michigan, Ann Arbor, MI 48109-1055, USA

[c]Department of Chemistry, University of Rochester, Rochester, NY 14627-0216, USA

Abstract

We present the synthesis, properties, and characterization of [Fe(T1Et4iPrIP)(NO)(H$_2$O)$_2$](OTf)$_2$ (**1**) (T1Et4iPrIP = Tris(1-ethyl-4-isopropyl-imidazolyl)phosphine) as a model for the nitrosyl adduct of gentisate 1,2-dioxygenase (GDO). The further characterization of [Fe(T1Et4iPrIP)(THF)(NO)(OTf)](OTf) (**2**) which was previously communicated (*Inorg. Chem.* **2014**, *53*, 5414) is also presented. The weighted average Fe-N-O angle of 162° for **1** is very close to linear (≥ 165°) for these types of complexes. The coordinated water ligands participate in hydrogen bonding interactions. The spectral properties (EPR, UV-vis, FTIR) for **1** are compared with **2** and found to be quite comparable. Complex **1** closely follows the relationship between the Fe−N−O angle and NO vibrational frequency which was previously identified for 6-coordinate {FeNO}^{7} complexes. Liquid FTIR studies on **2** indicate that the ν(NO) vibration position is sensitive to solvent shifting to lower energy (relative to the solid) in donor solvent THF and shifting to higher energy in dichloromethane. The basis for this behavior is discussed. The K_{eq} for NO binding in **2** was calculated in THF and found to be 470 M^{-1}. Density functional theory (DFT) studies on **1** indicate donation of electron density to the iron center from the π* orbitals of formally NO$^-$. Such a donation accounts for the near linearity of the Fe−N−O bond and the large ν(NO) value of 1791 cm^{-1}.

Introduction

Gentisate 1,2-dioxygenases (GDO) is an enzyme that catalyzes the ring scission reaction of gentisate (2,5-dihydroxybenzoate) between C1 and C2 to generate maleylpyruvate in the presence of oxygen. GDO plays a key role in the aerobic bacterial metabolism pathways (Scheme 1).[1] Although the structure of GDO from some bacteria have been confirmed,[1,2] the understanding of its catalytic cycle still remains unclear.[1-5] Recently, GDO from halophilic bacteria, *Martelella* strain AD-3, isolated from highly saline petroleum-contaminated soil, has been reported.[6]

GDO is a member of the Cupin superfamily of proteins which is characterized by two conserved metal-binding motifs.[7] The active site of GDO is comprised of two histidine residues in the first motif and a histidine residue in the second motif to form the 3His iron(II) binding site (Figure 1). Nonheme enzymes with ferrous active sites are usually spectroscopically silent and therefore difficult to characterize.[8,9] Nitric oxide (NO) is often used as an oxygen surrogate to probe the metal binding environment, spectroscopic and electronic properties, and requirements for catalytic turnover. GDO has been shown to have a low affinity for O_2 (and NO) in the absence of substrate.[3] This low affinity for electrophilic ligands is consistent with the known reversible binding of NO to GDO and other mononuclear ferrous enzymes[8] and therefore good synthetic analogues should also exhibit this behavior.
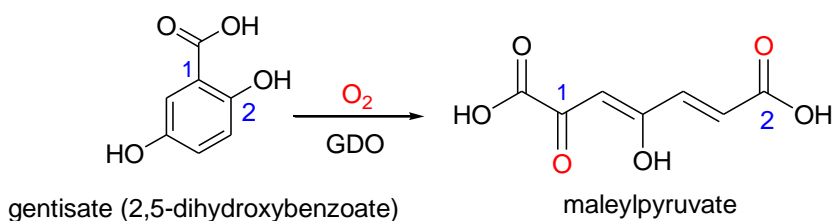
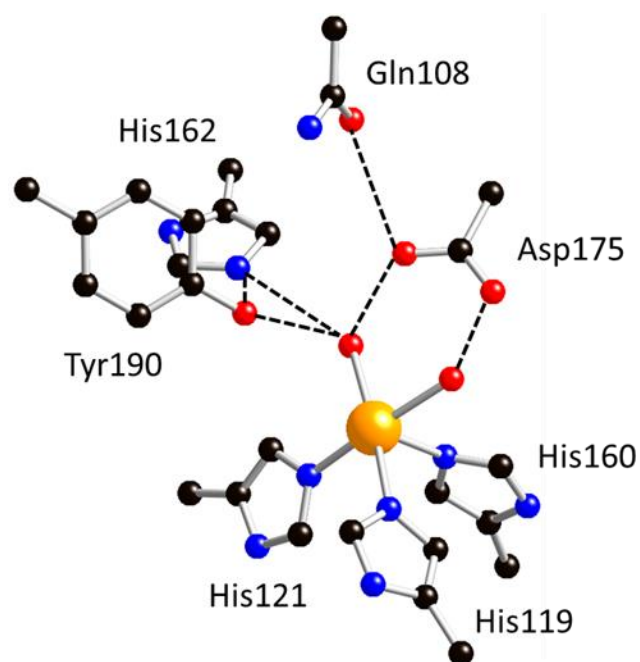**Scheme 1** Reaction catalyzed by Gentisate 1,2-dioxygenase (GDO).

Figure 1. Metal binding site for gentisate 1,2-dioxygenase (GDO, PDB 3BU7).

Here, we present a model complex for the nitrosyl adduct of GDO using [Fe(T1Et4iPrIP)(OTf)$_2$] (T1Et4iPrIP = Tris(1-ethyl-4-isopropyl-imidazolyl)phosphine, Scheme 2) as a model for the active site of GDO.[10]   Fielder and coworkers have recently published iron(II) complexes using similar trisimidazolyl phosphine ligands for the purpose of modelling the active sites of 3His enzymes.[11,12] Rahaman *et al.* have recently reported a structural and functional model for GDO, however an anionic trispyrazolyl ligand was employed and no adducts were investigated.[13]

T1Et4iPrIP   [Fe(T1Et4iPrIP)(OTf)$_2$]
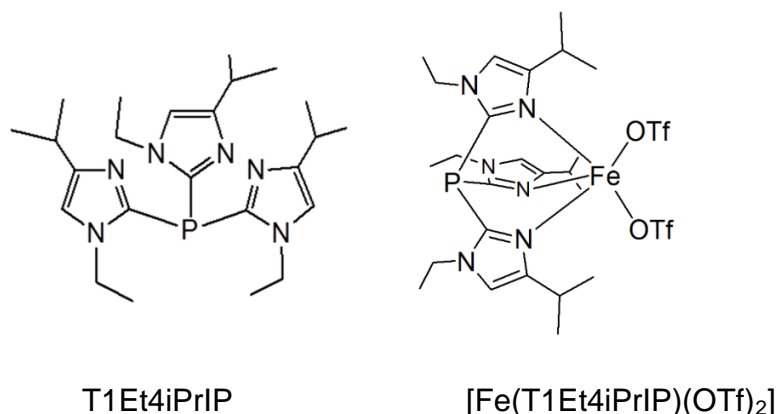
Scheme 2 Structure of ligand Tris(1-ethyl-4-isopropyl-imidazolyl)phosphine (T1Et4iPrIP) and [Fe(T1Et4iPrIP)(OTf)$_2$].[14]

Results and discussion

Synthesis and X-ray structure

The synthesis of [Fe(T1Et4iPrIP)(NO)(H$_2$O)$_2$](OTf)$_2$ (**1**) was achieved by reacting [Fe(T1Et4iPrIP)(THF)(NO)(OTf)](OTf) (**2**)[14] with 2.2 equiv water in dry THF and then diffusing pentane into this solution at 25 ºC under nitrogen. It is important to note that **1** cannot be prepared and isolated by adding 2.2 equiv water to [Fe(T1Et4iPrIP)(OTf)$_2$] followed by addition of NO or by using solvents other than THF (i.e. methanol, acetonitrile, dichloromethane). The NO ligand must be added first. The addition of water to **2** was monitored by UV-vis spectroscopy and revealed only minor changes in absorbance with slight increases in the 450 nm and 340 nm regions (Figure S1) and a slight decrease in the 240-270 nm region. Replacing the triflate and THF oxygen ligands with two water ligands would not be expected to result in large energy perturbations. Cooling a solution prepared in this manner to 5 ºC affords X-ray quality dark brown-black crystals after 2 days in good yield. The crystal structure was determine and the crystallogrphic parameters are given in Table S1 while selected metric parameters (as well as calculated) are contained in Table S2. The structure of **1** (shown in Figure

2) reveals iron bonded to an NO molecule along with three imidazole nitrogens in a facial manner along with two oxygens from water to afford a distorted octahedral geometry with NO occupying the apical position. The nitrosyl ligand in compound **1** is modeled as disordered over two positions (77:23). The dominant contributor has a Fe−N−O bond angle of 164.5(5)º, Fe−NO of 1.789(4), and N−O of 1.127(5) Å. The minor contributor has an angle of 152(3)º, Fe−NO of 1.770(14), and N−O of 1.114(16) Å. The weighted average yields an Fe-N-O angle of 162º, Fe−NO of 1.785, and N−O of 1.124 Å.
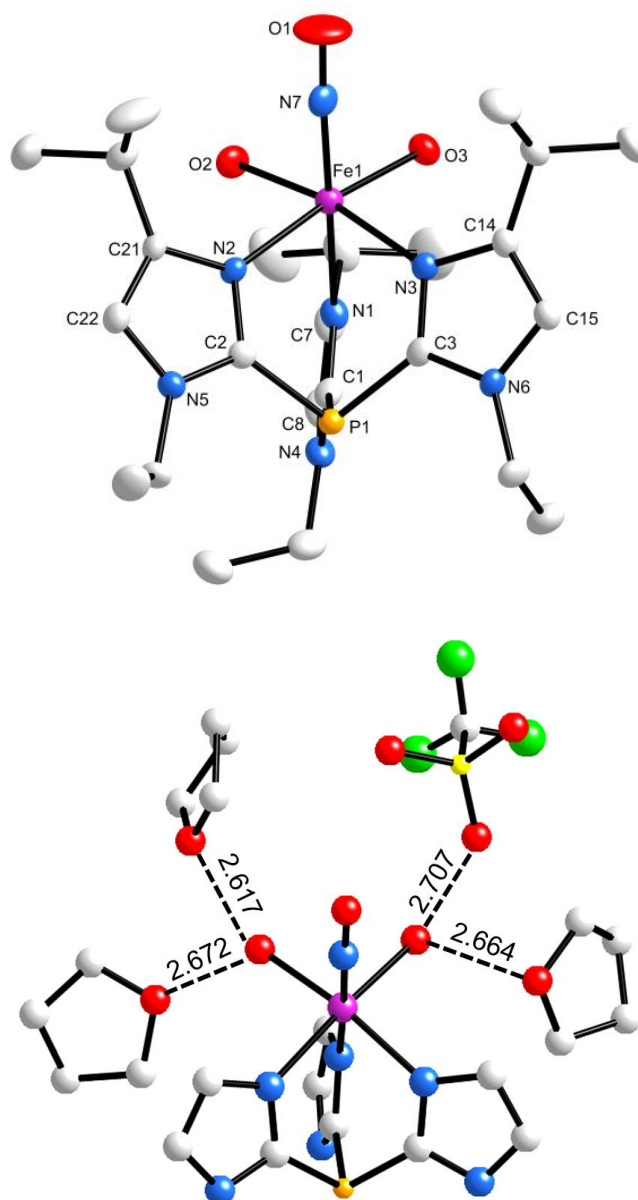
Figure 2. (top) X-ray structure (50% probability) of $[Fe(T1Et4iPrIP)(NO)(H_2O)_2]^{2+}$ (cation of **1**) and H-bonding between aqua ligands, triflate and THF molecules (Et and ^{i}Pr groups were removed from T1Et4iPrIP). H atoms have also been removed for clarity.

The aqua ligands in **1** participate in hydrogen bonding with a triflate and THF's (Figure 2, bottom). This aspect mimics the hydrogen bonding found in the GDO active site (Figure 1).

Spectroscopy

The UV-vis spectrum of **1** was acquired by adding 2.2 equiv water to **2** in THF (Figure S1). The absorption bands for **1** and **2** at $\lambda = 650$ nm are essentially identical while the band at $\lambda = 455$ nm (assigned to the Fe–NO LMCT band)[15,16] is slightly greater in intensity for **1**. On the other hand, the band for **1** at 269 nm is slightly lower in intensity compared to **2**.

The X-band EPR spectra for **1** and **2** were recorded at 4 K (1:2 Toluene:THF) and exhibit typical $S = 3/2$ signals with effective g values of ~4 and ~2 (Figure 3). These data are in accordance with the well-established electronic structure of non-heme ferrous nitrosyls, which show Fe(III)–NO⁻ ground states where the high-spin (HS) Fe^{3+} and NO^- ($S = 1$) are antiferromagnetically coupled.[9,16,17] The feature near the $g \sim 2$ region for **1** becomes more resolved (Figure 3, inset) when the temperature is increased to 15 K.
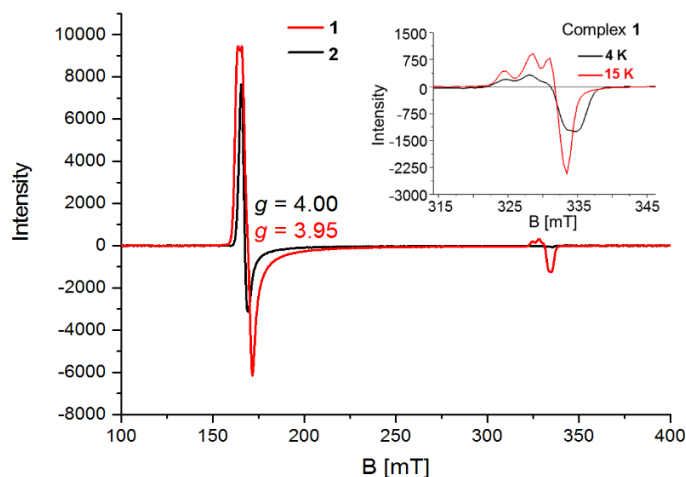

Figure 3. X-band EPR for [Fe(T1Et4iPrIP)(NO)(H₂O)₂](OTf)₂ (**1**) and [Fe(T1Et4iPrIP)(THF)-(NO)(OTf)](OTf) (**2**) in frozen THF solution at 4 K. EPR spectra in the $g \sim 2$ region for **1** at 4 K and 15 K are shown in the inset.

The magnetic circular dichroism (MCD) spectra of **2** in a polystyrene film were taken at magnetic fields ranging between 0-7 T (Figure 4). Since the optical properties of complexes **1**

and **2** are very similar, we decided to focus the MCD studies on compound **2**. The spectra suggest that a 6-coordinate {FeNO}[7] species exists.[18,19] The three main bands observed in the MCD data of **2** are attributed to electric dipole and spin-allowed $NO^- \pi^* \rightarrow Fe^{3+}$ LMCT bands, based on previous reports in the literature.[16] The three, broad bands observed in the MCD data of **2** can be Gaussian-deconvoluted into nine bands (see Figure 4), as listed in Table 1. This fit was obtained by simultaneously fitting the absorption spectrum of this complex, as also shown in Figure 4. In comparison, complex **1** displays very similar features as **2** (see Figure 4 and Table 1), with uniformly red-shifted bands and a slightly different intensity distribution in the 450 nm range. Nevertheless, this indicates that complexes **1** and **2** have very similar electronic structures.
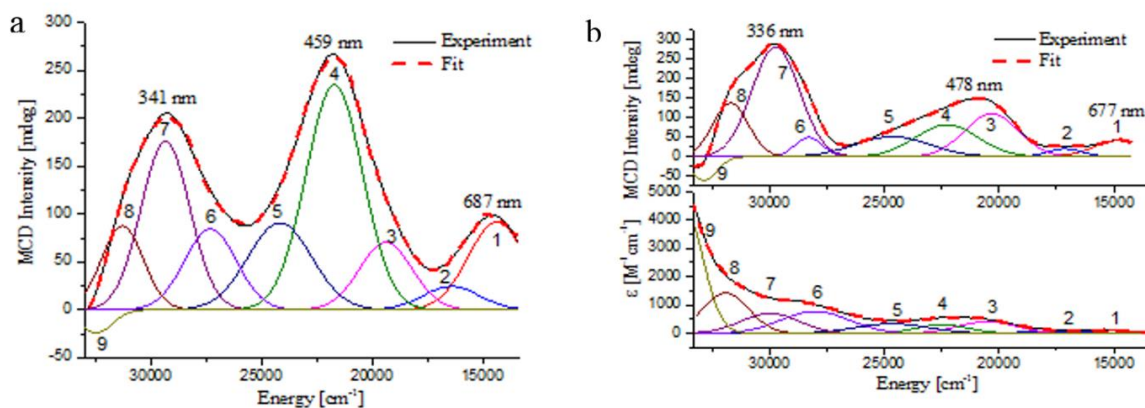

Figure 4. (a) Gaussian deconvolution of the 7T, 10K MCD spectrum of **1** using PeakFit. (b) Correlated Gaussian deconvolution of the MCD spectrum of **2** taken at 7 T, 10K (top), and the UV-vis spectrum of **2** taken at 298 K (bottom).

Table 1. Parameters for the MCD fit of **1** and for the correlated fit of the UV-Vis and MCD spectra of **2**.

	[Fe(T1Et4iPrIP)(NO)(H$_2$O)$_2$](OTf)$_2$ (**1**)		[Fe(T1Et4iPrIP)(THF)-(NO)(OTf)](OTf) (**2**)				
	MCD		**UV-vis**			**MCD**	
Band	**Energy (cm^{-1})**	**FWHM**	**Energy (cm^{-1})**	**ε (M^{-1} cm^{-1})**	**FWHM**	**Energy (cm^{-1})**	**FWHM**
1	14368	1292	14888	90	1009	14740	1098
2	16425	1271	17355	95	1323	17142	761
3	19381	1199	20517	416	1271	20271	1140
4	21710	1283	22485	300	1116	22052	1365
5	24178	1441	24671	339	1584	24395	1690
6	27318	1178	28033	777	1489	28302	535
7	29353	1104	30000	702	1266	29739	1087
8	31299	942	31931	1425	1005	31758	765
9	32485	733	33743	4444	809	32856	574

Vibrational spectroscopy was used to further characterize the nature of the Fe−N−O unit in **1**. The IR spectra (KBr pellet) of **1** exhibits ν(NO) at 1791 cm^{-1}. Interestingly, when the IR spectrum of **2** was monitored by ATR-IR in air, the 1831 cm^{-1} peak was observed along with a shoulder at 1791 cm^{-1}. Initially we suspected that oxidation of the iron could account for the position of the new peak, however it became clear that moisture in the air was coordinating to the iron and generating **1** in situ. Complete conversion on the day of the measurement was observed within 10 min (Figures 5 and S2). This is consistent with water being a better donor ligand than THF and triflate.[20,21]
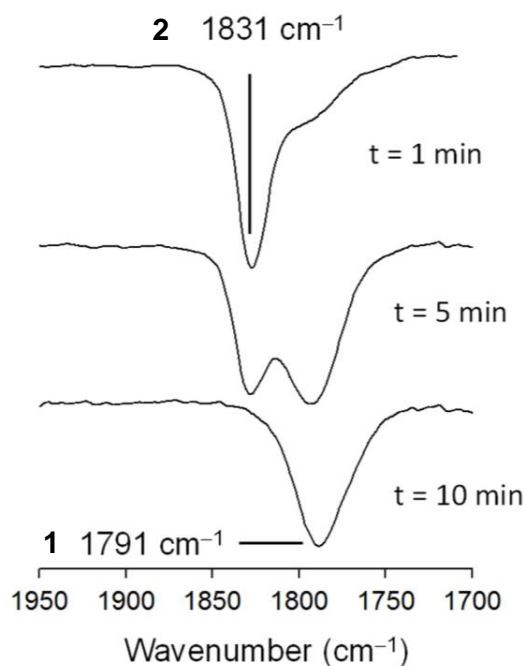
Figure 5. Fast conversion of **2** into **1** in the solid state in the presence of moist air as monitored by the shift in the ν(NO) stretch from 1831 to 1791 cm^{-1}, respectively, measured by ATR-IR.

Compound **1** appears to closely follow the relationship between the Fe−N−O angle and NO vibrational frequency which was previously identified for 6-coordinate compounds (Figure 6).[14] Although the NO group is slightly disordered in the X-ray structure, the IR spectrum clearly shows a single peak for ν(NO) indicating an averaging effect. The electronic/steric properties of the NO group are not influenced by other atoms since the nearest contact is 3.3 Å away. In fact if we consider 6-coordinate {FeNO}^{7} complexes where the nearest neighboring atom to the nitrosyl group is greater than 3.1 Å (Table 2), we see that the correlation between the Fe−N−O angle and the ν(NO) (Figure 6) remains.
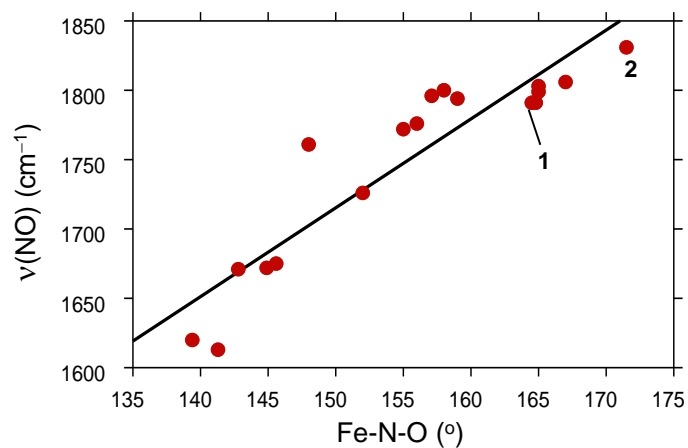
Figure 6. Correlation between Fe–N–O bond angle and ν(NO) for 6-coordinate complexes (See Table 4). Positions for complexes **1** and **2** are indicated. Linear fit (*R* = 0.92).

Table 2. Comparison of structural, electronic, and vibrational parameters for 6-coordinate Iron-nitrosyl {FeNO}^{7} complexes where the nearest neighboring atom to the nitrosyl group is > 3.1 Å.

Complex	Fe-NO (Å)	Fe–N–O (°)	N–O (Å)	ν(NO) (cm^{-1})	S	Ref
Free NO	------	------	-----	1875		[22]
[FeL(THF)(OTf)(NO)](OTf)^a (**2**)	1.765	168.6	1.146	1831^r	3/2	[14]
[FeL(THF)(OTf)(NO)](OTf)^a (**2**)	1.763	174.4	1.153	1831^r	3/2	[14]
[Fe(dipic)(H$_2$O)$_2$(NO)]^b	1.76	167	1.14	1806^s	3/2	[23]
[Fe(bnida)(H$_2$O)$_2$(NO)]^c	1.78	165	1.13	1803^s	3/2	[23]
[Fe(brbnida)(H$_2$O)$_2$(NO)]^d	1.80	158	1.09	1800^s	3/2	[23]
[Fe(H$_2$O)$_2$(NO)(oda)]^e	1.77	165	1.15	1799^s	3/2	[23]
[Fe(TMPzA)Cl(NO)](BPh$_4$)^f	1.725	157.1	1.15	1796^r	3/2	[15,24]
[Fe(TPA)(BF)(NO)]ClO$_4$^{g}	1.72	159	1.15	1794^r	3/2	[15]
[FeL(THF)(NO)(H$_2$O)$_2$](OTf)$_2$^{a} (**1**)	1.789	164.5	1.127	1791^r	3/2	This work
{[Fe(H$_2$O)$_4$]}Fe(NO)(nta)}$_2$]$_{n/n}$^{h}	1.752	164.8	1.152	1791^r	3/2	[25]
[Fe(EDTA)(NO)]^i	1.78	156	1.1	1776^t	3/2	[9]
[Fe(H$_2$O)$_2$(ida)(NO)]^j	1.78	155	1.11	1772^s	3/2	[23]
[Fe(edda)(H$_2$O)(NO)]^k	1.775	148	1.163	1761^r	3/2	[25]
[Fe(BMPA-Pr)Cl(NO)]^l	1.783	152	1.154	1726^r	3/2	[26]
[Fe(Me$_2$bpb) (NO)]^m	1.714	145.6	1.18	1675^r	1/2	[27]
[Fe(bztpen)NO](OTf)$_2$^{n}	1.733	142.8	1.184	1671^s	-----	[28]
[Fe(N4Py)(NO)](BF$_4$)$_2$^{o}	1.732	144.9	1.157	1672^s	1/2	[29]
[Fe(pyN$_4$)(NO)]Br$_2$^{p}	1.737	139.4	-----	1620^r	1/2	[30]
[Fe(PaPy$_3$) (NO)]$^{+q}$	1.752	141.3	1.19	1613^r	1/2	[31]

^{a}L = tris(1-ethyl-4-isopropyl-imidazolyl)phosphine, ^{b}dipic = dipicolinate, ^{c}bnida = *N*-benzyliminodiacetate, ^{d}brbnbida = N-4-bromobenzyliminodiacetate, ^{e}oda = oxodiacetate, ^{f}TMPzA = tris(3,5-dimethylpyrazol-1-ylmethyl)amine, ^{g}TPA = tris(2-pyridylmethyl)amine and BF = benzoylformate, ^{h}nta = nitrilotriacetate, ^{i}EDTA = ethylenediamine-*N,N,N',N'*-tetraacetate, ^{j}ida = iminodiacetate, ^{k}edda = ethylenediamine-*N,N'*-diacetate, ^{l}BMPA-Pr = *N*-propanoate-*N,N*-bis(2-pyridylmethyl)amine, ^{m}Me$_2$bpb = *N,N'*-bispyridinecarboxamido-4,5-dimethylbenzenediamine, ^{n}bztpen = *N*-benzyl-*N,N',N'*-tris(2-pyridylmethyl)ethylenediamine), ^{o}N4Py = 1,1-di(pyridin-2-yl)-*N,N*-bis(pyridin-2-ylmethyl)methanamine, ^{p}pyN$_4$ = 2,6-bis(1',3'-diamino-2'-methylprop-2'-yl)pyridine, ^{q}PaPy$_3$ = *N*-[*N,N*-bis(2-pyridylmethyl)aminoethyl]-2-pyridinecarboxamide. ^{r}KBR pellet, ^{s}ATR-IR, ^{t}Raman.

Recent studies on {FeNO}^{7} complexes that undergo spin-crossover also appear to confirm the trend shown in Figure 6.[32,33]

Solution FTIR studies were conducted on [Fe(T1Et4iPrIP)(OTf)$_2$] and complex **2**. The spectra in THF are shown in Figure 7 (a) and (b), respectively. The spectrum of **2** in CH$_2$Cl$_2$ is shown in Figure 7(c). The results of these studies indicate that the ν(NO) vibration is highly sensitive to solvent. In comparison to **2** measured in the solid state (ν(NO) = 1831 cm^{-1}), we see that the ν(NO) for **2** in THF solution appears at 1820 cm^{-1} while **2** in CH$_2$Cl$_2$ has ν(NO) = 1844 cm^{-1}. In THF the lower vibrational energy is consistent with increased electron density donated to the highly Lewis acidic iron center. This could be explained by THF solvent exchanging with the coordinated OTf$^-$. This results in decreased β-electron donation from the nitrosyl π* orbital[14] resulting in a decreased bond order for the NO group. It can thus be argued that when **2** is measured in CH$_2$Cl$_2$ that the species generated contains weaker donors (compared to THF and OTf$^-$ ligands found in the solid state). We suggest that when **2** is dissolved in CH$_2$Cl$_2$ that the bound THF is replaced by OTf$^-$ (due to electrostatic effects in the noncoordinating low relative polarity solvent). This results in an overall weaker donor set, a more Lewis acidic iron center, and a stronger N−O bond (thus a higher ν(NO)). Using ^{19}F NMR it is possible to assess the binding mode for OTf$^-$. It has been shown for high spin iron(II) complexes that when OTf$^-$ is bound in a terminal manner it gives rise to a single resonance at −14 ppm, whereas the resonance for unbound OTf$^-$ occurs near −80 ppm.[34,35] To provide insight into the solution behavior and OTf$^-$ coordination mode for **1** and **2** we conducted ^{19}F NMR experiments on **1** and **2** in d_8-THF and **2** in CD$_2$Cl$_2$ (Figure 8). As can be seen, **1** exhibits a slightly broadened resonance at −57.6 ppm in d_8-THF suggesting that while the primary formulation [Fe(T1Et4iPrIP)(H$_2$O)$_2$](OTf)$_2$ is correct, some exchange between an aqua and triflate ligand is occuring. Complex **2**, on the other hand has a much broader resonance at −45.4 ppm which also suggests an exchange process with the OTf$^-$ equilibrium shifted more towards the bound form. Addition of 0.7 equiv OTf$^-$

((Bu$_4$N)(OTf)) to **2** results in a shift in the peak to −53.5 ppm consistent with a larger amount of unbound OTf⁻. In the case of **2** dissolved in CD$_2$Cl$_2$, we see a peak that is shifted downfield indicating an exchange process with a larger amount of bound OTf⁻. This possibly indicates that the THF ligand is lost and that the exchange process is between [Fe(T1Et4iPrIP)(NO)(OTf)$_2$] and [Fe(T1Et4iPrIP)(NO)(OTf)]$^+$ and OTf⁻ (or [Fe(T1Et4iPrIP)(NO)(THF)(OTf)]$^+$ and OTf⁻).

(a)

[Fe(T1Et4iPrIP)(OTf)$_2$] in THF

(b)

2 in THF

1820 cm⁻¹

(c)

2 in CH$_2$Cl$_2$

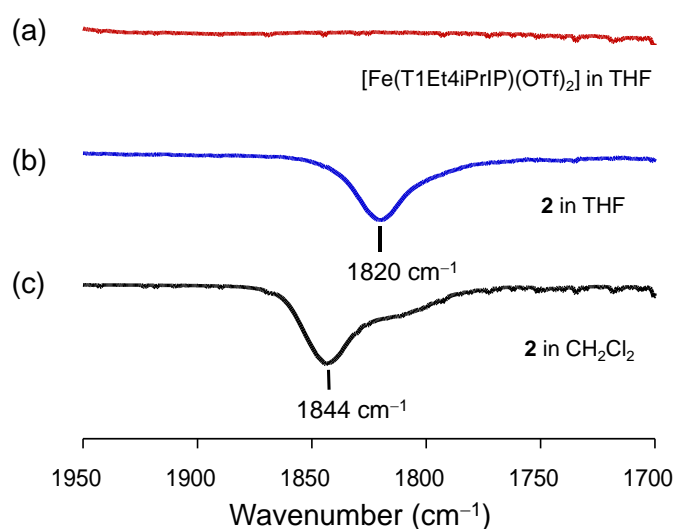1844 cm⁻¹

1950   1900   1850   1800   1750   1700

Wavenumber (cm⁻¹)

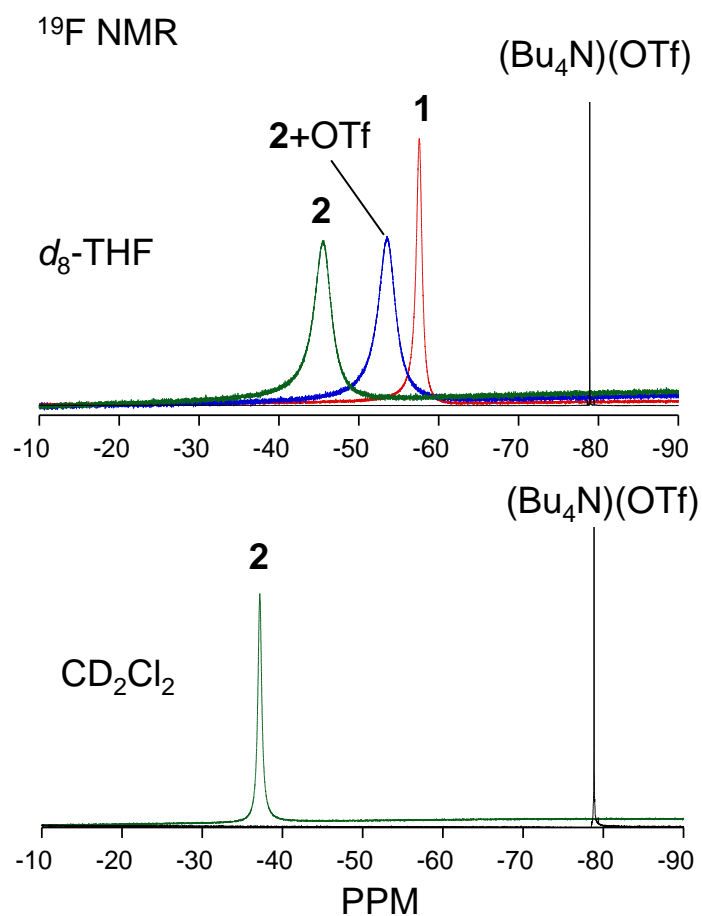**Figure 7**. Liquid FTIR measurements on (a) [Fe(T1Et4iPrIP)(OTf)$_2$] in THF, (b) **2** in THF, and (c) **2** in CH$_2$Cl$_2$.

Figure 8. ^{19}F NMR of **1**, **2**, and **2** + 0.7 equiv (Bu$_4$N)(OTf) in d_8-THF (Top) and **2** in CD$_2$Cl$_2$ at 376.5 MHz and 25 °C. The peak near −80 ppm is for (Bu$_4$N)(OTf) dissolved in the respective solvents.

Equilibrium studies

To further characterize the properties of complex **2**, we studied the LFe + NO $\leftrightarrow$ LFeNO equilibrium process using UV-vis spectroscopy by titrating a known amount of [Fe(T1Et4iPrIP)(OTf)$_2$] into a solution of NO (7 mM) in THF at 25 ºC (Figure 9). Equation 1 was employed to fit the empirical data. The study revealed the equilibrium constant (K_{eq}) to be 470 M^{-1} which is comparable to values found in similar studies.[36]

$$A_x = A_0 + \frac{(A_\infty - A_0)K_{eq}[Fe^{II}]}{1 + K_{eq}[Fe^{II}]}$$

(1)
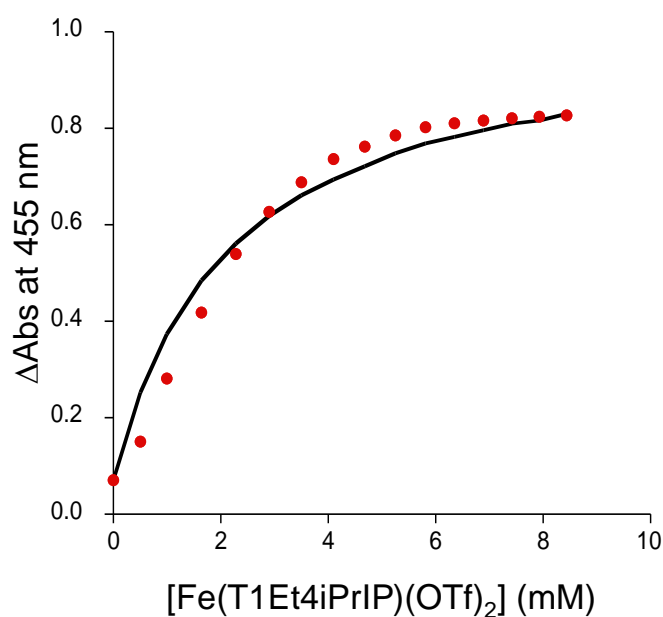
Figure 9. Change in absorbance at 455 nm for the reaction of [Fe(T1Et4iPrIP)(OTf)₂] with NO. [NO] = 7 mM, T = 25 ºC.

Computational Studies

To characterize the electronic structure of **1** in direct comparison to that of **2**,[14] we performed DFT calculations. The UB3LYP/6-31G(d)-optimized structure of **1** is in very good agreement with experimental values. Calculated metric parameters are included in Table S2 (in brackets) and show Fe−N bond distances to be within 0.033 Å of the experimental bond lengths. The calculated Fe−O$_{aqua}$ bond distances are substantially longer (0.141 and 0.174 Å) compared to experimental values. This could be due to the presence of H-bonding in the experimental structure, which was not included in the calculation or the small basis set used in the calculation.

The optimized Fe−NO distance is 1.793 Å in close agreement with the weight-averaged experimental value (1.785 Å). The Fe−N−O weighted average angle of 162º (calc: 159.3º) and N−O bond distance 1.124 Å (calc: 1.116 Å) are also in good agreement with calculated values. The calculated ν(NO) of 1889 cm^{-1} (no scaling) is quite large compared to the experimental value (1791 cm^{-1}), however, overestimation of the N-O stretch with UB3LYP is typical for this functional.[37] This allows one to gain insights into the electronic structure of the FeNO group. Close inspection of the molecular orbital (MO) diagram of **1** indicates a high spin (HS) Fe(III)−NO$^-$ bonding scheme description.[9] The α-spin MO diagram reveals that all iron d orbitals are singly occupied. With the Fe−NO vector corresponding to the z axis, the d_{xz} and d_{yz} orbitals are unable to form back-bonding with the two unoccupied α-π* orbitals of NO. The β-spin MO diagram (Figure 10), however, contains unoccupied iron d orbitals, while the β-π* orbitals of NO are now occupied, consistent with the NO$^-$ ($S = 1$) description of the NO ligand. Occupied β-π* orbitals of NO are ideally positioned to donate into the empty β-spin d_{xz} and d_{yz} orbitals of iron. The degree of this interaction can be reasonably estimated by considering the antibonding combinations β144 (34% d_{yz/z^2}, 57% π*) and β145 (29% d_{xz}, 60% π*), which clearly illustrate significant iron d-orbital and NO π* character[38] (See Figure 10). The π donation from NO$^-$ into the iron β-d_{xz} and β-d_{yz} orbitals is important and a similar result was observed for the anhydrous analogue ([Fe(T1Et4iPrIP)(NO)(THF)(OTf)](OTf) (**2**).[14] To summarize, the NO$^-$ ligand functions as a strong β-spin π-donor ligand in **1**.[26,39]
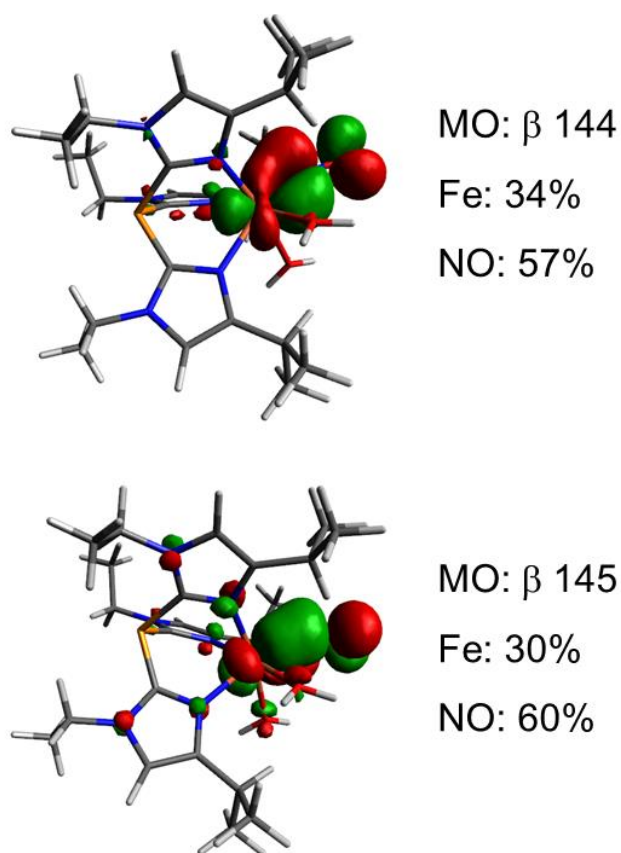
Figure 10. β-spin isosurface MO diagram for iron *d* orbitals and π* orbitals of NO for [Fe(T1Et4iPrIP)(NO)(H₂O)₂]²⁺ (cation of **1**).

For **1**, the calculated spin density distribution for Fe is +3.90 while NO has a value of −01.16. This is in clear agreement with the above mentioned electronic description for the FeNO unit. For **2**, the values were slightly more disparate (Fe +3.93, NO −1.15) which is consistent with the observed parameters for **2** (shorter Fe−NO bond (1.777 Å), more linear Fe−N−O angle (169.5°), larger ν(NO) (1831 cm⁻¹)). Lehnert has previously indicated that decreasing the negative charge on the iron leads to the iron's increased ability to accept electron density from bound NO⁻.[26]

Summary and conclusions

In summary, we have synthesized an accurate model for the nitrosyl adduct of GDO. The model complex ([Fe(T1Et4iPrIP)(NO)(H$_2$O)$_2$](OTf)$_2$, **1**) binds nitric oxide with a bent Fe−N−O group. We compared the spectroscopic properties of **1** with those of the anhydrous analogue ([Fe(T1Et4iPrIP)(THF)(NO)(OTf)](OTf), **2**). It was determined that the nitrosyl structural and vibrational characteristics were strongly influenced by the electron donating ability of accessory ligands. In **1**, the water ligands provide more electon density to the iron center compared to triflate and THF ligands present in **2**. This results in lower Lewis acidity for the iron in **1** and concomitant higher π* electon density in the nitrosyl group corresponding to a lower energy ν(NO). These results are supported by DFT studies on **1**. The K_{eq} was determined to be 470 M^{-1} for the LFe + NO ↔ LFeNO process in **2**.

Experimental section

Anhydrous THF, pentane, and ether were obtained using a solvent purification system (Innovative Technologies, Inc.). [Fe(T1Et4iPrIP)(OTf)$_2$] was prepared according to a published method.[10] Nitric oxide gas (99.5%, Praxair) fitted with a stainless steel regulator was first passed through an ascarite/P$_2$O$_5$ column and then through a −130 ºC trap (pentane/liquid nitrogen slush bath) followed by activated 4A molecular sieves.

[Fe(T1Et4iPrIP)(H$_2$O)$_2$(NO)](OTf)$_2$·3THF (1·3THF). Nitric oxide was bubbled into a freshly prepared solution of [Fe(T1Et4iPrIP)(OTf)$_2$] (40 mg, 0.050 mmol) in anhydrous THF (1 mL) in a 25 mL Teflon-stoppered solvent storage flask with a rubber septum affixed to the side arm under positive nitrogen pressure. After NO was bubbled into the solution for 2 min, the clear colorless

solution became dark brown. The Teflon stopper was reattached and through the septum was added 2.2 equiv H_2O (2.0 µL, 0.110 mmol) in anhydrous THF (1 mL) and anhydrous pentane (2 mL) under nitrogen. The mixture was placed at 5 ℃ and after several days, yellow-brown needles were deposited. Yield: 25 mg (58.0%). FT-IR [ν(NO)]: 1791 cm^{-1} (KBr). UV-vis (THF) [λ_{max}, nm (ε, M^{-1}, cm^{-1})]: 269 (23,150), 345 (1230, sh), 457 (650), 650 (175). Magnetic measurements, μ_{eff} (polycryst, 297 K): 4.60 μ_B.

Physical methods

A Cary 50 UV-vis spectrophotometer was used to collect optical spectra. FT-IR spectra were acquired on a Varian 3100 Excalibur Series and a Bruker ATR Alpha P spectrometer. X-Band electron paramagnetic resonance spectra were obtained on a Bruker X-band EMX spectrometer equipped with an Oxford Instruments liquid helium cryostat. Spectra were recorded on frozen 1:2 toluene:THF solutions of **1** and **2**, using 20.5 mW microwave power, 100 kHz field modulation, and 1 G modulation amplitude. NMR spectra were monitored at 25 °C on a Brüker Avance II 400 MHz instrument. ^{1}H NMR peaks were referenced to TMS while ^{19}F NMR peaks were referenced to CF_3CO_2H (−76.56 ppm). Magnetic measurements on polycrystalline samples at 298 K were performed using a Johnson-Matthey magnetic susceptibility balance.

X-ray crystallography

Complex **1** was crystallized by cooling a THF-pentane solution of **1** at 5 °C. A yellow-brown needle (0.30 x 0.20 x 0.06 mm^3) was attached onto the tip of a 0.1 mm diameter glass capillary tube or fiber and mounted on a Bruker SMART APEX II CCD Platform diffractometer for a data collection at 100.0(5) K.[40] A preliminary set of cell constants and an orientation matrix were

calculated from reflections harvested from three orthogonal wedges of reciprocal space. The full data collection was carried out using MoK$_\alpha$ radiation (graphite monochromator) with a frame time of 60 seconds and a detector distance of 3.98 cm. A randomly oriented region of reciprocal space was surveyed: six major sections of frames were collected with 0.50º steps in ω at six different ϕ settings and a detector position of −38º in 2θ. The intensity data were corrected for absorption.[41] Final cell constants were calculated from the xyz centroids of 4008 strong reflections from the actual data collection after integration.[42] See Table S1 for additional crystal and refinement information. The nitrosyl ligand is modeled as disordered over two positions (77:23). Data for **1** (CCDC: 966460) has been deposited. These data can be obtained free of charge via http://www.ccdc.ac.uk/conts/retrieving.html, or from the Cambridge Crystallographic Data Centre, 12 Union Road, Cambridge CB2 1EZ, UK; fax: (.44) 1223-336-033; or e-mail: deposit@ccdc.cam.ac.uk.

MCD spectroscopy

MCD spectra of **1** were obtained on a mull of fine powder of **1** suspended in silicone oil. MCD spectra of **2** were obtained in thin polystyrene (PS) films. The films were prepared by dissolving the complex and PS pellets in dichloromethane, followed by slow evaporation of the solvent in the glovebox. The PS films were placed between two quartz plates which were mounted on a copper sample holder. MCD spectra were recorded using a setup that consists of an OXFORD SM4000 cryostat and a JASCO J-815 CD spectropolarimeter. The SM4000 consists of a split pair superconducting magnet providing horizontal magnetic fields of 0–7 T in a low boil-off helium cryostat. The light source of the J-815 is an air cooled xenon lamp. The detector system corresponds to two interchangeable head-on photomultiplier tubes. Samples are

loaded into a 1.5–300 K variable temperature insert (VTI), which offers access to the sample via four optical windows made from Spectrosil B quartz.

Computational studies

Quantum chemical calculations providing energy minimized molecular geometries, molecular orbitals (HOMO-LUMO), and vibrational spectra for **1** were carried out using density functional theory (DFT) as implemented in the GAUSSIAN09 (Rev. C.01) program package.[43] We employed the functional B3LYP. The basis set used was 6-31G(d).[444] The solvent (THF) was simulated with the default method implemented in Gaussian 09 which uses the Polarizable Continuum Model. Full ground state geometry optimization was carried out without any symmetry constraints. Only the default convergence criteria were used during the geometry optimizations. The initial geometry was taken from the crystal structure coordinates in the quintet state. Optimized structures were confirmed to be local minima (no imaginary frequencies for both cases). Theoretical and experimental geometric parameters are given in Table S2. Molecular Orbitals were generated using Avogadro[45] (an open-source molecular builder and visualization tool, Version1.1.0. http://avogadro.openmolecules.net/).

Acknowledgements

Keywords: Iron(II) nitrosyl complexes · Imidazole ligand · X-ray Crystallography · Magnetic Circular Dichroism · Density Functional Calculations ·

Supporting Information

Crystallographic information for **1**, UV-vis and FT-IR spectra for **1** and **2** (PDF, 31 pages) is available. Crystallographic data for **1** (CCDC 1548010) has been deposited. These data can be obtained free of charge via http://www.ccdc.ac.uk/conts/retrieving.html, or from the Cambridge Crystallographic Data Centre, 12 Union Road, Cambridge CB2 1EZ, UK; fax: (.44) 1223-336-033; or E-mail: deposit@ccdc.cam.ac.uk.

[1] M. A. Adams, V. K. Singh, B. O. Keller and Z. Jia, *Mol. Microbiol.* **2006**, *61*, 1469-1484.

[2] J. Chen, W. Li, M. Wang, G. Zhu, D. Liu, F. Sun, N. Hao, X. Li, Z. Rao and X. C. Zhang, *Protein Sci.* **2008**, *17*, 1362-1373.

[3] M. R. Harpel and J. D. Lipscomb, *J. Biol. Chem.* **1990**, *265*, 22187-22196.

[4] E. Eppinger, S. Burger and A. Stolz, *FEMS Microbiol. Lett.* **2016**, *363*, fnv211.

[5] E. Eppinger and A. Stolz, *Protein Eng. Des. Sel.* **2017**, *30*, 57-65.

[6] L. Huang, H. Hu, H. Tang, Y. Liu, P. Xu, J. Shi, K. Lin, Q. Luo and C. Cui, *Sci. Rep.* **2015**, *5*, 14307.

[7] S. Fetzner, *Appl. Environ. Microbiol.* **2012**, *78*, 2505-2514.

[8] A. M. Orville, V. J. Chen, A. Krauciunas, M. R. Harpel, B. G. Fox, E. Munck and J. D. Lipscomb, *Biochemistry* **1992**, *31*, 4602-4612.

[9] C. A. Brown, M. A. Pavlosky, T. E. Westre, Y. Zhang, B. Hedman, K. O. Hodgson and E. I. Solomon, *J. Am. Chem. Soc.* **1995**, *117*, 715-732.

[10] E. Korendowych, A. L. Crown, M. S. Harbuz, D. S. Jessop, S. L. Lightman and J. R. Kirwan, *Rheumatology* **2001**, *40*, 22-22.

[11] A. E. Baum, S. V. Lindeman and A. T. Fiedler, *Eur. J. Inorg. Chem.* **2016**, 2455-2464.

[12] M. M. Bittner, S. V. Lindeman, C. V. Popescu and A. T. Fiedler, *Inorg. Chem.* **2014**, *53*, 4047-4061.

[13] R. Rahaman, B. Chakraborty, T. K. Paine, *Angew. Chem., Int. Eng. Ed.* **2016**, *55*, 13838-13842.

[14] J. Li, A. Banerjee, P. L. Pawlak, W. W. Brennessel and F. A. Chavez, *Inorg. Chem.* 2014, *53*, 5414-5416.

[15] Y. M. Chiou and L. Que *Inorg. Chem.*, **1995**, *34*, 3270-3278.

[16]   T. C. Berto, A. L. Speelman, S. Zheng and N. Lehnert, *Coord. Chem. Rev.* **2013**, *257*, 244-259.

[17]   T. E. Westre, A. Dicicco, A. Filipponi, C. R. Natoli, B. Hedman, E. I. Solomon and K. O. Hodgson, *J. Am. Chem. Soc.* **1994**, *116*, 6757-6768.

[18]   T. A. Jackson, E. Yikilmaz, A. F. Miller and T. C. Brunold, *J. Am. Chem. Soc.* **2003**, *125*, 8348-8363.

[19]   N. Lehnert, *J. Inorg. Biochem.* **2012**, *110*, 83-93.

[20]   C. Diver and Lawrence, G. A., *J. Chem. Soc. Dalton Trans.* **1988**, 931-944.

[21]   R. Díaz-Torres and S. Alvarez, *Dalton Trans.* **2011**, *40*, 10742-10750.

[22]   G. B. Richter-Addo and P. Legzdins, *Metal Nitrosyls*, Oxford University Press, New York, 1992.

[23]   M. Wolf and P. Klufers, *Eur. J. Inorg. Chem.* **2017**, 303-2312.

[24]   C. R. Randall, Y. Zang, A. E. True, L. Que, J. M. Charnock, C. D. Garner, Y. Fujishima, C. J. Schofield and J. E. Baldwin, *Biochemistry* **1993**, *32*, 6664-6673.

[25]   B. M. Aas and P. Klufers, *Eur. J. Inorg. Chem.* **2017**, 2313-2320.

[26]   T. C. Berto, M. B. Hoffman, Y. Murata, K. B. Landenberger, E. E. Alp, J. Y. Zhao and N. Lehnert, *J. Am. Chem. Soc.* **2011**, *133*, 16714-16717.

[27]   M. J. Rose, A. K. Patra, M. M. Olmstead and P. K. Mascharak, *Inorg. Chim. Acta* **2010**, *363*, 2715-2719.

[28]   T. Nebe, A. Beitat, C. Wurtele, C. Ducker-Benfer, R. van Eldik, C. J. McKenzie and S. Schindler, *Dalton Trans.* **2010**, *39*, 7768-7773.

[29] A. C. McQuilken, Y. Ha, K. D. Sutherlin, M. A. Siegler, K. O. Hodgson, B. Hedman, E. I. Solomon, G. N. Jameson and D. P. Goldberg, *J. Am. Chem. Soc.* **2013**, *135*, 14024-14027.

[30] J. P. Lopez, F. W. Heinemann, R. Prakash, B. A. Hess, O. Horner, C. Jeandey, J. L. Oddou, J. M. Latour and A. Grohmann, *Chem. Eur. J.* **2002**, *8*, 5709-5722.

[31] A. K. Patra, J. M. Rowland, D. S. Marlin, E. Bill, M. M. Olmstead and P. K. Mascharak, *Inorg. Chem.* **2003**, *42*, 6812-6823.

[32] L. Pineiro-Lopez, N. Ortega-Villar, M. C. Munoz, G. Molnar, J. Cirera, R. Moreno-Esparza, V. M. Ugalde-Saldivar, A. Bousseksou, E. Ruiz and J. A. Real, *Chemistry* **2016**, *22*, 12741-12751.

[33] A. C. McQuilken, H. Matsumura, M. Durr, A. M. Confer, J. P. Sheckelton, M. A. Siegler, T. M. McQueen, I. Ivanovic-Burmazovic, P. Moenne-Loccoz and D. P. Goldberg, *J. Am. Chem. Soc.* **2016**, *138*, 3107-3117.

[34] D. W. Blakesley, S. C. Payne and K. S, Hagen, *Inorg. Chem.* **2000**, *39*, 1979-1989.

[35] J. England, R. Gondhia, L. Bigorra-Lopez, A. R. Petersen, A. J. P. White and G. J. P. Britovosek, *Dalton Trans.* **2009**, 5319-5334.

[36] S. Begel, R. Puchta, J. Sutter, F. W. Heinemann, L. Dahlenburg, R. van Eldik, *Inorg. Chem.* **2015**, *54*, 6763-6775.

[37] C. van Stappen, N. Lehnert, *Inorg. Chem.* **2018**, *57*, 4252-4269.

[38] M. Radon, E. Broclawik, K. Pierloot, *J. Phys. B* **2010**, *114*, 1518-1528.

[39] A. L. Speelman, N. Lehnert, *Angew. Chem. Int. Ed.* **2013**, *52*, 12283-12287

[40] *APEX2, version 2011.4-1; Bruker AXS: Madison, WI, 2011*.

[41]   *Sheldrick, G. M. SADABS, version 2008/1; University of Göttingen: Göttingen, Germany, 2008.*

[42]   *SAINT, version 7.68A; Bruker AXS: Madison, WI, 2009.*

[43]   M. J. Frisch, G. W. Trucks, H. B. Schlegel, G. E. Scuseria, M. A. Robb, J. R. Cheeseman, G. Scalmani, V. Barone, B. Mennucci, G. A. Petersson, H. Nakatsuji, M. Caricato, X. Li, H. P. Hratchian, A. F. Izmaylov, J. Bloino, G. Zheng, J. L. Sonnenberg, M. Hada, M. Ehara, K. Toyota, R. Fukuda, J. Hasegawa, M. Ishida, T. Nakajima, Y. Honda, O. Kitao, H. Nakai, T. Vreven, J. A. Montgomery, Jr., J. E. Peralta, F. Ogliaro, M. Bearpark, J. J. Heyd, E. Brothers, K. N. Kudin, V. N. Staroverov, T. Keith, R. Kobayashi, J. Normand, K. Raghavachari, A. Rendell, J. C. Burant, S. S. Iyengar, J. Tomasi, M. Cossi, N. Rega, J. M. Millam, M. Klene, J. E. Knox, J. B. Cross, V. Bakken, C. Adamo, J. Jaramillo, R. Gomperts, R. E. Stratmann, O. Yazyev, A. J. Austin, R. Cammi, C. Pomelli, J. W. Ochterski, R. L. Martin, K. Morokuma, V. G. Zakrzewski, G. A. Voth, P. Salvador, J. J. Dannenberg, S. Dapprich, A. D. Daniels, O. Farkas, J. B. Foresman, J. V. Ortiz, J. Cioslowski and D. J. Fox, *Gaussian09, Revision C.01, Gaussian Inc., Wallingford CT, 2010.*

[44]   G. A. Petersson and M. A. Al-Laham, *J. Chem. Phys.* **1991**, *94*, 6081-6090.

[45]   M. Hanwell, D. Curtis, D. Lonie, T. Vandermeersch, E. Zurek and G. Hutchison, *J. Cheminf.* **2012**, *4*, 1-17.

We report a model for the iron-nitrosyl adduct of gentisate dioxygenase ($[Fe(T1Et4iPrIP)(NO)(H_2O)_2](OTf)_2$, **1**). Complex **1** is synthesized by the addition of 2 equiv water to $[Fe(T1Et4iPrIP)(THF)(NO)(OTf)](OTf)$ (**2**). A correlation between the solid-state Fe-N-O angle and $\nu(NO)$ is elaborated and the K_{eq} in THF for the reversible binding of NO to **2** is reported. The influence of solvent on the value of $\nu(NO)$ for **2** is also discussed.
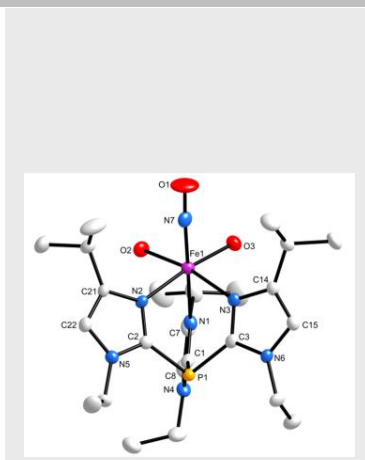
Bioinorganic Iron-Nitrosyl Models

Atanu Banerjee, Jia Li, Amy L. Speelman, Corey J. White, Piotr L. Pawlak, William W. Brennessel, Nicolai Lehnert, Ferman A. Chavez*

Page No. – Page No.

A Structural Model for the Iron-Nitrosyl Adduct of Gentisate Dioxygenase